Electron Tunneling at the TiO_2/Substrate Interface Can Determine Dye-Sensitized Solar Cell Performance

Sven Rühle‡ and David Cahen*

Department of Materials and Interfaces, Weizmann Institute of Science, Rehovot 76100, Israel

Received: May 28, 2004; In Final Form: August 16, 2004

The electric potential distribution in dye-sensitized solar cells plays a major role in the operation of such cells. Models based on a built-in electric field which sets the upper limit for the open circuit voltage (V_{oc}) and/or the possibility of a Schottky barrier at the interface between the mesoporous wide band gap semiconductor and the transparent conducting substrate have been presented. We show that $I-V$ characteristics in the dark and upon illumination are very well explained by electron tunneling, rather than transport over a Schottky barrier, at this interface. Our calculations, based on tunnel currents, show that a discontinuity of the conduction band at the TiO_2/FTO interface, rather than a built-in electric field, suffices for efficient electron transfer through this interface, and, thus, for efficient operation of this type of solar cell. Clearly, this will hold only if the photoinduced electrostatic potential barrier between the transparent conducting substrate and the mesoporous wide band gap semiconductor drops over a region that is sufficiently narrow to allow efficient tunneling through it.

Introduction

Dye-sensitized solar cells (DSSCs) are a promising, potentially low cost alternative to conventional p−n-junction solar cells. They consist of a dye-covered, mesoporous TiO_2 film deposited on a conducting transparent substrate (usually F-doped tin oxide, FTO), which is immersed into an I^-/I_3^- redox electrolyte. While in the laboratory such systems can reach solar to electric conversion efficiencies of about 10%,[1] they are not yet manufactured on a large scale, mainly due to technical problems such as sealing. Solid-state devices, in which the liquid electrolyte is replaced by a solid-state hole conductor, including so-called ETA (Extreme Thin Absorber layer) cells, are a promising alternative, but their efficiency (∼4%) is still significantly below that of the liquid electrolyte cells.[2−4]

Further improvement of liquid- and solid-state DSSCs requires understanding of the electric and chemical potential distributions in the dark and upon illumination. Initially it was accepted that the V_{oc} of DSSCs is limited by the energy difference between the bottom of the TiO_2 conduction band (E_{CB}) and the redox potential (E_{redox}) of the electrolyte (the so-called kinetic model). Some years ago it was proposed that the V_{oc} is limited by a built-in electric field at the TiO_2/FTO interface and that such a field is essential for the operation of DSSCs (the so-called junction model).[5] Subsequently, it was suggested that one can merge both models, so that a built-in potential does not necessarily limit the V_{oc}[6,7] but might have a strong effect on the fill factor.[7]

It appears that what happens at the FTO/TiO_2 interface is the origin of disagreements about the working principle of DSSCs. In the following we briefly review the existing models, emphasizing their (dis)agreements, especially in as far as these concern the FTO/TiO_2 interface. We distinguish two types of DSSCs, one that consists of the mesoporous TiO_2 film that is directly sintered onto the FTO substrate (Figure 1a) and the other that uses an additional dense, compact TiO_2 layer (Figure 1h). Such a layer has a width of some tens of nanometers to avoid direct contact between the electrolyte and the conductive substrate and to suppress recombination from the FTO substrate. We analyze the electrostatic potential distribution at this interface for systems without compact layer and introduce an analytical expression for electron tunneling through an electrostatic barrier. With the aid of numerically calculated current−voltage ($I-V$) characteristics in the dark and under illumination, we then discuss the influence of the tunnel barrier on the fill factor, and on the V_{oc}.

Theoretical Background

The Kinetic Model. Electron injection from the excited dye state into the TiO_2 conduction band (CB) is a very fast process in DSSCs (on the *femto*second scale[8]), while the reduction of the oxidized dye by the redox electrolyte's I^- ions occurs in about 10^{-8} seconds.[9] Recombination of photoinjected CB electrons with oxidized dye molecules or with the oxidized form of the electrolyte redox couple (I_3^- ions) occurs in *micro*seconds, and, thus, is orders of magnitude slower than the injection and recharging process of the dye.[9] The high efficiency of charge separation at the TiO_2/dye/electrolyte interface is explained by the huge difference in these rate constants, for electron and hole injection into the TiO_2 CB and redox electrolyte, respectively, on one hand, and for recombination of CB electrons with oxidized dye molecules or I_3^- ions, on the other hand. These are kinetic parameters, which is the origin for the models' name.

Photoinjection increases the electron density in the TiO_2 network, shifting the electron's quasi-Fermi level E_{Fn} (nonequilibrium analogue of electrochemical potential of electrons) toward the TiO_2 CB (Figure 1c) while E_{redox} remains nearly unchanged due the high concentration of redox species.[10] E_{Fn} is defined as the chemical potential, μ_e, plus the electrostatic potential, φ, times the electron charge, $-q$:

$$E_{Fn} = \mu_e - q\varphi \quad (1)$$

* Address correspondence to this author. E-mail: david.cahen@weizmann.ac.il.
‡ E-mail: sven.ruehle@weizmann.ac.il.

10.1021/jp047686s CCC: $27.50
Published on Web 10/22/2004

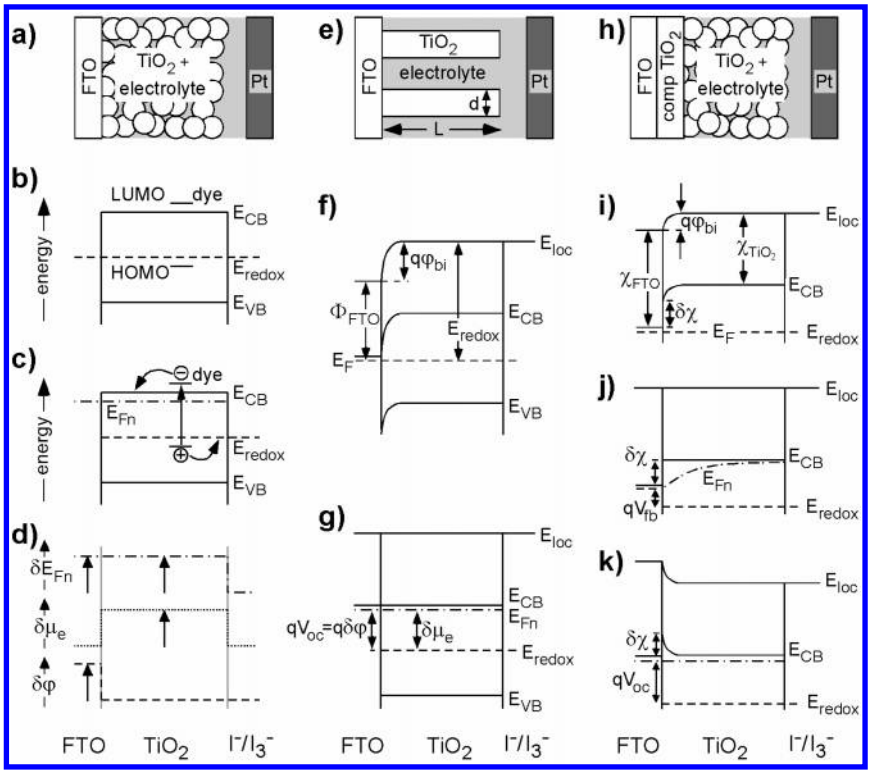

Figure 1. (a) Scheme of a mesoporous, nanocrystalline DSSC without the compact underlayer. (b) Corresponding energy band diagram in the dark according to the "kinetic" model. The energy level of the lowest unoccupied molecular orbital (LUMO) of the dye is located above the TiO_2 conduction band edge (E_{CB}) while the highest occupied molecular orbital (HOMO) is at lower energy than the redox potential (E_{redox}) of the electrolyte. (c) Same as panel b upon illumination at open circuit voltage V_{oc}. Photoinjected electrons shift the quasi-Fermi level, E_{Fn}, toward E_{CB}, and the FTO substrate takes on the potential of the mesoporous TiO_2. Often the kinetic model does not treat the electric field explicitly so that no local vacuum level is depicted. (d) Three schematic potential energy diagrams that show the central role of the FTO/TiO_2 contact for the DSSC at V_{oc}. Shown are the light-induced changes (δE_{Fn}, $\delta\mu_e$, and $\delta\varphi$) of the quasi-Fermi level E_{Fn}, the chemical potential μ_e, and the electrostatic potential φ, at V_{oc}. E_{Fn} is shifted up in the TiO_2 film and in the FTO substrate (top); inside the film only the chemical potential is changed (due to negligible band edge movement), while the change in electrostatic potential occurs at the FTO/TiO_2 contact (bottom). Each diagram is with respect to a separate, arbitrary reference. The same diagrams result, irrespective of which model is used, the "kinetic" or the "junction" one. (e) Simplified geometric structure, used to calculate the electrostatic potential distribution according to the "junction" model. The mesoporous TiO_2 film is approximated by cylinders with a diameter d of the nanoparticles and a length L equivalent to the film thickness. (f) Energy band diagram according to the "junction" model, showing the postulated built-in field φ_{bi} at the FTO/TiO_2 interface in the dark, caused by a difference in the substrate work function Φ_{FTO} and E_{redox}. (g) Same as panel f upon illumination, at V_{oc}, which flattens the bands. The shift of E_{Fn} inside the porous TiO_2 structure is due to a chemical potential shift $\delta\mu_e$, which is converted into an electrostatic potential shift, $\delta\varphi$, at the FTO/TiO_2 interface (shown as an upward shift of E_{loc} and the FTO bands). The shift corresponds to the measured photovoltage. (h) Scheme of DSSC with compact TiO_2 underlayer (~50−100 nm thick) used for measurements to support the thermionic emission model.[14] (i) Band diagram for the scheme of panel h in the dark. The difference in CB levels of the FTO and the TiO_2 is due to a built-in field and to a band offset caused by a difference in the electron affinity, χ, of the two materials. For simplicity the VB band is not shown. (j) Same as panel i, upon illumination. The built-in field is neutralized at the flat band potential, V_{fb}. (k) Same as panel i; for voltages $> V_{fb}$ a barrier exists at the FTO/TiO_2 interface, which can only be crossed by electrons with sufficient kinetic energy, until V_{oc} is reached, as shown in the band diagram.

The light-generated increase of electrons in the TiO_2 network affects μ_e strongly, while φ remains nearly unchanged.[11] Therefore, band edge movement in the mesoporous structure is usually neglected. The chemical potential shift is converted at the FTO/TiO_2 interface into a change of the electrostatic potential of the FTO (as shown schematically in Figure 1d at V_{oc}). The energy difference between E_{Fn} (at the FTO contact) and E_{redox} corresponds to the photovoltage of the DSSC,[12] i.e., in the kinetic model V_{oc} is limited by the energy difference between E_{CB} and E_{redox}.[13]

The kinetic model usually does not discuss explicitly the electrostatic potential distribution, whether in the dark or under illumination (the local vacuum level E_{loc} is usually not depicted in energy band diagrams, see, e.g., Figure 1, panels b and c), but was explicitly addressed by the junction model.[5]

The Junction Model. The junction model is based on an electrostatic approach and agrees with the kinetic model that no electric field is present in most of the TiO_2 film. However, in contrast to the kinetic model, it requires a built-in electric field *in the dark* at the FTO/TiO_2 interface. According to the model this field is essential for the operation of DSSCs and sets an upper limit to the maximum attainable V_{oc}. The difference between E_{redox} and the work function of the FTO substrate (Φ_{FTO}) together with insufficient electrostatic screening inside the TiO_2 are the origin of the built-in potential. The electrostatic potential distribution inside the TiO_2 has been calculated for a simplified geometry,[6,15] where the mesoporous TiO_2 film was approximated by TiO_2 cylinders, oriented normal to the FTO substrate, with a diameter d equal to the particle diameter and a length L corresponding to the film thickness (Figure 1e). Band diagrams for the DSSC in the dark and upon illumination according to the junction model are shown in Figure 1, panels f and g, respectively.

A problem of the junction model is the lack of experimental evidence for the postulated correlation between the V_{oc} and the energy difference between the substrate work function and the redox potential. Measurements of the V_{oc} on systems, where the FTO was replaced by other conducting substrates with

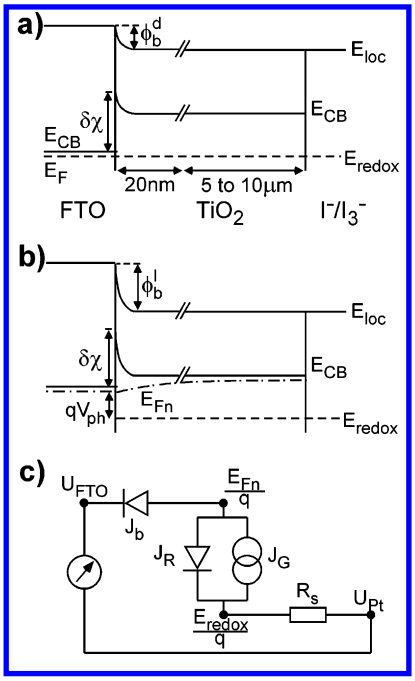

Figure 2. (a and b) Energy band diagrams for the tunnel-junction model based on experimental data from Kelvin probe measurements. An electrostatic barrier ϕ_b^d of about 100 meV is present in the dark (a). This barrier increases for any applied photovoltage ($\phi_b^l = \phi_b^d + qV_{ph}$) as depicted in part b. The potential drop appears in the first layer of TiO_2 particles (~20 nm) in contact with the FTO. (c) Equivalent circuit that includes a diode to model the barrier at the FTO/TiO_2 interface. The difference between the potentials U_{FTO} and U_{Pt} is what can be measured experimentally ($V_{ph} = U_{FTO} - U_{Pt}$). In addition we show where the equivalents of the electrochemical potentials, E_{Fn}/q and E_{redox}/q, are applied in this equivalent circuit.

different work functions, did not show the predicted effect on the V_{oc}. In contrast the V_{oc} seemed to be nearly independent of the work function of the substrate.[7,16]

The Thermionic Emission Model. A numerical model for DSSCs,[6] as well as calculations based on an equivalent circuit,[7,17] showed that a built-in field does not necessarily limit the V_{oc}, if thermionic emission at the FTO/TiO_2 interface is taken into account. We will refer to this approach as the thermionic emission model. $I-V$ characteristics of DSSCs, with a compact TiO_2 underlayer between the conductive substrate and the mesoporous network (schematically shown in Figure 1h), were analyzed with the simple equivalent circuit depicted in Figure 2c, assuming a Schottky barrier at the FTO/TiO_2 interface.[7,17] The photocurrent was represented by a current source (J_G), and recombination was described by a regular diode equation (J_R). A resistor, R_S, was connected in series to account for transport losses in the electrolyte.

Calculations showed[17] that the Schottky barrier can result in an S-shaped $I-V$ curve, significantly decreasing the fill factor while leaving the V_{oc} unaffected. These calculations were supported by experiments (on cells with a compact TiO_2 layer between the FTO and the porous TiO_2), where the Schottky barrier height at the conducting substrate/TiO_2 interface was systematically changed.[7]

Energy band diagrams with a built-in field and a CB discontinuity $\delta\chi$ at the FTO/TiO_2 interface are shown in Figure 1i,j,k. The CB discontinuity is the result of a difference in FTO and TiO_2 electron affinities, i.e., $\chi_{FTO} \neq \chi_{TiO_2}$. Figure 1i shows the situation in the dark ($E_F = E_{redox}$), Figure 1j that at flat band potential ($V = V_{fb}$), and Figure 1k that at open circuit ($V = V_{oc}$). The maximum photovoltage that can be achieved is limited by the energy difference between E_{CB} and E_{redox}, just as in the kinetic model.

The problem of the equivalent circuit-based analyses that include a Schottky barrier is their inability to model the dark $I-V$ characteristics correctly with physically reasonable parameters. Built-in voltages of several hundreds of millielectronvolts are required for a good fit with measured data, which seems to be rather high according to our experimental data. In the following section we show that DSSCs can operate *without* built-in field, if electron tunneling is considered at the FTO/TiO_2 interface. To emphasize the effect of the transport mechanism at the interface we present simulated $I-V$ curves based on the same equivalent circuit as that used in the thermionic emission model.[7,17]

The Tunnel-Junction Model. *The FTO/TiO_2 Interface.* In accordance with the junction model we assume that the electrostatic potential distribution at the FTO/TiO_2 interface is defined by the redox potential of the I^-/I_3^- electrolyte and the FTO work function. Contact potential difference (CPD) measurements were used to determine E_{redox} (~4.75 eV) and Φ_{FTO} in ambient atmosphere (~4.85 eV). The measurements were done in a home-built setup with a commercial Kelvin probe (Besocke Delta Phi, Jülich, Germany). While the measurement of Φ_{FTO} was done in a standard fashion, a special liquid cell was used to measure E_{redox}.[18] This measurement method has the advantage that both energy levels, the FTO work function and the redox potential, were measured with respect to the same reference (the Kelvin probe). As the simplest approach we assume that Φ_{FTO} does not change significantly after the FTO is immersed into the electrolyte. From the CPD data we derive that the built-in potential difference at the FTO/TiO_2 interface is ~100 mV, but with a polarity *opposite* to the built-in field, proposed by the junction and thermionic emission model.[19] This electrostatic barrier, ϕ_b, increases with applied photovoltage upon solar cell operation. Energy band diagrams, consistent with our measured data, are shown for the dark (Figure 2a) and upon illumination for some photovoltage, $V_{ph} < V_{oc}$ (Figure 2b).

It the following we show that the electrostatic barrier ϕ_b at the FTO/TiO_2 interface does not necessarily affect the $I-V$ characteristics of DSSCs. To do so we introduce an analytical expression for electron tunneling through the barrier ϕ_b (Figure 2a,b) and restrict the analysis to DSSCs without compact underlayer.

The electrostatic potential distribution in the TiO_2 particles in contact with the FTO substrate was calculated by using boundary conditions, similar to those proposed by the junction model, viz. a constant electrostatic potential at the TiO_2 particle surface in contact with the electrolyte (a potential that differs from the constant potential of the FTO substrate), and a linear potential drop across the Helmholtz layer at the FTO/electrolyte interface. We used a somewhat more realistic structure (Figure 3a) than the simplified TiO_2 rod geometry.[5,6,15] The Laplace equation inside the TiO_2 nanocrystals was solved with the above-mentioned boundary conditions. Figure 3a shows the electrostatic potential distribution (equipotential lines) inside the first two layers of TiO_2 particles in contact with the FTO substrate for a particle diameter of 25 nm, an interface diameter at the contact area with neighboring particles or the FTO substrate of 15 nm, and a Helmholtz layer width of 1.4 Å (see Figure 3a, insert). Figure 3a shows that the entire potential drop appears within the first layer of TiO_2 particles in contact with the FTO substrate while, already all through the second layer of particles, the potential is that of the electrolyte.

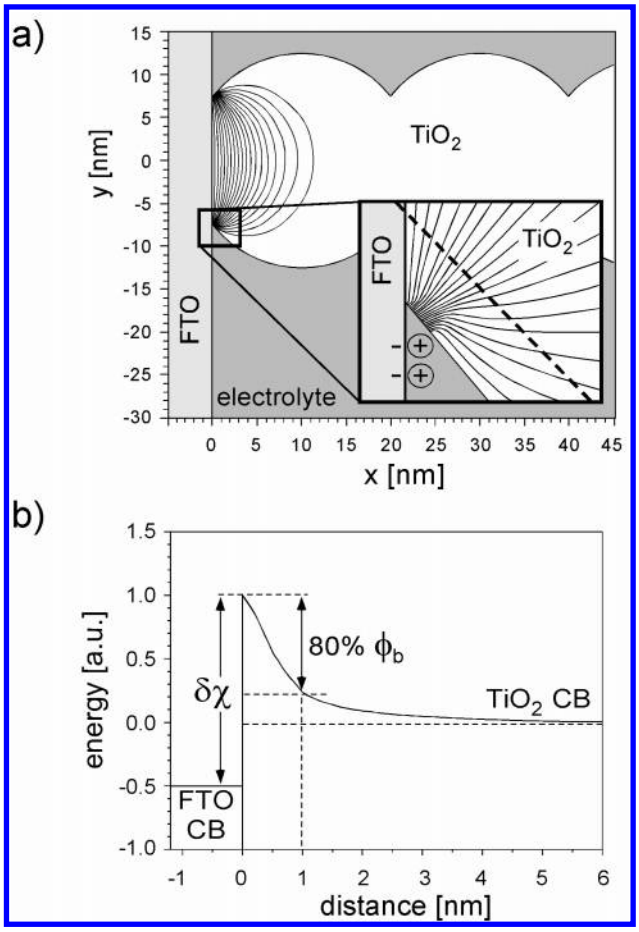

Figure 3. (a) Electrostatic potential distribution, depicted by equipotential lines, for the first two layers of particles in contact with the FTO substrate. The particle radius is 25 nm and the cross section radius between the TiO_2 nanoparticle and FTO substrate is 15 nm. The insert shows the magnified view of the potential distribution close to the three-component FTO/TiO_2/electrolyte interface including the Helmholtz layer. (b) The CB along the dashed line (shown in the insert of panel a) as a function of distance from the substrate. Some 80% of the potential barrier drop occurs within the first nanometer.

The CB as a function of the distance from the FTO substrate along the dashed line, close to the three-component FTO/TiO_2/electrolyte interface (see Figure 3a, insert), is plotted in Figure 3b. It shows that 80% of the potential drop appears over a distance of about 1 nm, while the potential drop in the center of the particle appears over several nanometers, as can be seen from the equi-potential lines in Figure 3a. Thus, efficient electron tunneling is only considered at that part of the FTO/TiO_2 interface that is close to the electrolyte where the barrier width is sufficiently thin. In the calculations presented below this was taken into account by an effective interface area, smaller than the geometric interface area.

The Tunnel Current at the FTO/TiO_2 Contact. We start from an analytical expression for tunneling through an asymmetric barrier between metal contacts and derive an extended expression for the semiconductor/barrier/metal interface case, applicable to our situation. Even though the FTO substrate is a degenerate semiconductor and not a metal, we will treat it here as a metal due to its high conductivity. The tunnel barrier is represented by that part of the TiO_2 film at the interface where the bands are bent because of the electrostatic potential difference between the FTO substrate and the electrolyte. For our analysis we simplify the shape of the real tunnel barrier

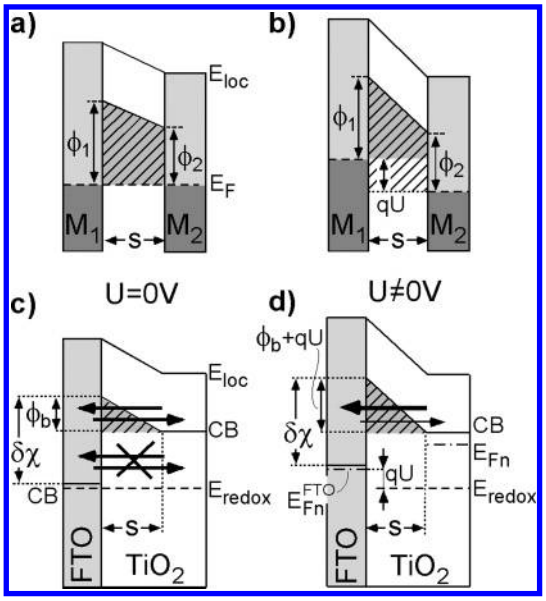

Figure 4. (a and b) Energy level diagrams showing tunnel barriers for the metal (M_1)/insulator/metal (M_2) system at zero bias (a) and at some applied bias with a net electron current from M_1 to M_2 (b). (c and d): Extension of panels a and b to a metal/barrier/semiconductor system, where the degenerate FTO semiconductor is treated as a metal so that the energy difference between the FTO quasi-Fermi level and the FTO CB is neglected. The barrier is due to the bending of the TiO_2 CB (cf. Figure 3b) and is approximated by a triangular barrier (hatched on grey background).

(shown in Figure 3b), to a triangular barrier of constant thickness, shown in Figure 4c.

For a trapezoidal barrier, connected between two metal contacts M_1 and M_2, the tunnel current is given by[20−22]

$$J_t = A[\bar{\gamma}_1(U)\exp(B\sqrt{\bar{\gamma}_1(U)}) - \bar{\gamma}_2(U)\exp(B\sqrt{\bar{\gamma}_2(U)})] \quad (2)$$

with constants $A = q/2\pi h\beta s^2$ and $B = -4\pi\beta s\sqrt{2m_e^*}/h$, which contain Planck's constant h, the elementary charge q, the barrier width s, the effective electron mass m_e^*, and a correction factor β, which is close to 1 so that it will be neglected in the following. The first term in eq 2 contains an average barrier height $\bar{\gamma}_1(U) = (\phi_1 + \phi_2 - qU)/2$ and describes the current from metal contact M_1 into M_2, while the second term describes the current from M_2 into M_1 with an average barrier height $\bar{\gamma}_2(U) = (\phi_1 + \phi_2 + qU)/2$, which is schematically depicted in panels a and b of Figure 4 at thermal equilibrium and at applied bias, respectively. Equation 2 is based on the WKB approximation and the simplification of the real barrier shape by an average barrier height $\bar{\gamma}$.[20]

To extend eq 2 to the FTO/barrier/TiO_2 interface we introduce the TiO_2 band edge positions into the energy diagram and assume that only CB electrons participate in the tunnel process. Electron transfer from TiO_2 gap states into the FTO or vice versa is neglected,[7,17] as shown schematically by the crossed-out arrows in Figure 4c. From Figure 4c and d one can see that the accessible barrier for electron tunneling reduces to a triangle so that the average barrier height for electron tunneling from the FTO into the TiO_2 is identical with the barrier height for electron tunneling from the TiO_2 into the FTO. The bottom of the barrier is located above the Fermi level in contrast to the metal/barrier/metal case. To take this into account we multiply both terms from eq 2 by the Boltzmann factor, so that the tunnel current from the TiO_2 into the FTO or vice versa is modified by the electron density in the FTO and TiO_2, respectively. Thus the tunnel current through an FTO/barrier/TiO_2 is described by

$$J_t = CA\bar{\gamma}(U)\exp\left(B\sqrt{\bar{\gamma}(U)}\right)\left[\exp\left(\frac{\delta\chi - \phi_b + qU}{k_B T}\right) - \exp\left(-\frac{E_{CB} - E_{Fn}}{k_B T}\right)\right] \quad (3)$$

where the potential-dependent average barrier height is given by $\bar{\gamma}(U) = (\phi_b + qU)/2$ with the built-in potential ϕ_b, as shown in Figures 2a, 3b, 4c, and 4d. We note again that the built-in field has a polarity opposite to that proposed by the junction model. The scaling factor C takes into account that electron tunneling is only relevant in that part of the FTO/TiO_2 interface area close to the electrolyte, where the electrostatic barrier is relatively thin. The first term in the square brackets is the Boltzmann factor that describes the probability to have thermally activated CB electrons in the FTO at the bottom of the barrier, while the second term describes the probability to find electrons in the TiO_2 CB. Note that E_{CB}, E_{Fn}, $\delta\chi$, and ϕ_b are negative quantities. Upon cell operation the difference between the forward (from the TiO_2 into FTO) and backward current (from the FTO into the TiO_2) is caused by the difference in the Boltzmann factors in the TiO_2 and the FTO. This is in contrast to what is the case for the tunnel current at metal/barrier/metal interfaces, where that difference is due to a difference between the tunnel barrier for backward and forward currents. As a result the net current in Figure 4d has a sign opposite to that in Figure 4b, even though the electrostatic potential difference is the same.

$I-V$ curves were calculated for the equivalent circuit depicted in Figure 2c where the characteristics of the junction diode (J_b) are given by eq 3. The photo- and recombination currents in the TiO_2 used for the calculations are defined as

$$J_R = J_0\left[\exp\left(\frac{E_{Fn} - E_{redox}}{k_B T}\right) - 1\right] - J_G \quad (4)$$

with the same ideality factor n_{if}, saturation current J_0, and the generation current J_G as in ref 17 (in contrast to ref 17 we scaled the current density at the FTO/TiO_2 junction according to the effective interface area and did not increase J_0 and J_G).

$I-V$ curves were calculated with the MATLAB code with the parameters used for the simulations summarized in Table 1. The series resistance R_S was chosen to be infinitely small to emphasize the effect of the tunnel barrier on the $I-V$ characteristics. Dark and light $I-V$ characteristics are plotted in Figure 5. For the calculations it was assumed that 40% of the geometric FTO area is in contact with TiO_2 particles and 60% is in contact with the electrolyte. Furthermore, we considered electron tunneling only at that part of the FTO/TiO_2 interface which is not more than 0.5 nm away from the electrolyte, which means that the effective tunnel area per particle is ~13% of the real particle/FTO interface area, so that the scaling factor C was 0.052.

Discussion

Figure 5 shows that the $I-V$ characteristics remain unaffected by the tunnel barrier if the CB offset between the TiO_2 and the FTO is 0.95 eV and the width of the effective tunnel barrier is 0.9 nm or less. For thicker barriers a decrease in the fill factor is observed and the $I-V$ curves show some S-shape for barrier widths of 1.2 nm or more. We mention that the input parameters for the calculations included estimations, like the effective tunnel area at the FTO/TiO_2 interface, and small variations of other parameters (like the energy level of the TiO_2 CB or the dark barrier height ϕ_b^d) have a strong effect on the tunnel current. It is the aim of the simulations to demonstrate that DSSCs without a built-in field can show high light to electric conversion efficiencies with use of a reasonable set of material parameters, when electron tunneling is introduced into the system. $I-V$ characteristics based on thermionic emission at the FTO/TiO_2 interface did not show any significant photocurrent in the external circuit, when calculated with the same set of input parameters (not shown). Therefore the thermionic emission model requires a built-in electric field, which promotes electron transfer from the TiO_2 into the FTO, in contrast to the tunnel-junction model.

TABLE 1: Parameters Used To Calculate the Current−Voltage Curves Shown in Figure 5

J_0	4×10^{-8} mA/cm^2	$E_{CB}(TiO_2)$	−4.00 eV
n_{if}	1.5	E_{redox}	−4.85 eV
T	300 K	$\delta\chi$	−0.95 eV
J_G	10 mA/cm^2	ϕ_b^{dark}	−0.10 eV
R_S	0 Ω cm^2	m_e*	5.6m_e

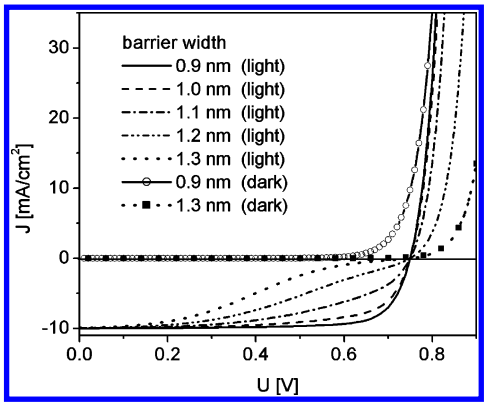

Figure 5. Calculated $I-V$ curves for an equivalent circuit with a tunnel barrier at the FTO/TiO_2 interface. While the $I-V$ curve is unaffected by the tunnel barrier for a barrier width of 0.9 nm, it shows a significant decrease of the fill factor for barrier widths of 1.1 nm or more. The parameters used to calculate the current−voltage curves are given in Table 1.

The solid $I-V$ curve in Figure 5 does not differ significantly from that of an ideal solar cell without a barrier. This might lead to the wrong conclusion that there is no difference between the tunnel-junction model and the kinetic model as presented in ref 12. We emphasize that the model from ref 12 assumes that the chemical potential is completely converted into an electrostatic potential at the FTO/TiO_2 interface *at any voltage*. This is not the case in the presence of a barrier for electron transfer from the TiO_2 into the FTO, even though the $I-V$ curves are similar. For a fundamental understanding of the working principle of the cells this is essential because it demonstrates that DSSCs can work perfectly well without any built-in field. In this they differ fundamentally from p−n-junction cells.[23]

As DSSCs with and without a compact TiO_2 underlayer are reported in the literature, we note that the potential distribution presented in Figure 3 was calculated for a system *without* underlayer. A light-induced electrostatic barrier, which drops across the 50 to 100 nm thick compact layer, is not thin enough for efficient electron tunneling. However, electron tunneling in systems with underlayer might be possible if the electrostatic potential barrier drops over a very narrow region inside the compact underlayer. This could be the case if Li^+ ions (electrolytes mostly used contain Li^+) intercalate into the compact layer,[24] get sufficiently close to the FTO substrate, and are charge-compensated by electrons in the FTO substrate. We note that Li^+ intercalation would also change the electrostatic

potential distribution at the mesoporous TiO_2/FTO interface and thus increase the effective interface area for electron tunneling.

Including electronic states in the TiO_2 band gap is another possibility to explain DSSC operation for devices with a barrier across the compact TiO_2 underlayer. The tunnel-junction model does not include gap states, which can be involved in electron hopping through the barrier. Hopping may well be the dominant transport mechanism through compact TiO_2 layers. Additionally charge accumulation in the gap states might cause band bending in the compact layer[25] and thus narrow the barrier, which would be beneficial for electron tunneling. However, this would require a rather high density of gap states.

Conclusions

Experimental work function data of the FTO substrate and E_{redox} of the I^-/I_3^- couple indicate that an electrostatic field is present in the dark at the FTO/TiO_2 interface. This field creates an energy barrier for electron transfer from the TiO_2 into the FTO. This is in contrast to previous models,[5,7,17] which proposed an electrostatic built-in field in the dark that *promotes* electron transfer into the FTO substrate. In our model the barrier increases with applied photovoltage, which can give rise to a nonlinear contact resistance that affects significantly the performance of DSSCs. While the V_{oc} is limited by the energy difference between E_{CB} and E_{redox}, the band line-up at the FTO/TiO_2 interface can have a significant influence on the fill factor. In contrast to proposed band structures that involve a built-in electric field that promotes electron collection of the FTO substrate, we show that DSSCs can give high efficiencies in the absence of such a built-in field. Analysis of the electrostatic potential distribution at the mesoporous TiO_2/FTO interface reveals that the potential barrier width is approximately 1 nm, thin enough for electron tunneling. An analytical expression for the tunnel current was derived, under the assumption that electronic gap states are not involved in the process. Our analysis is restricted to DSSCs *without* the compact TiO_2 blocking layer that is often introduced between the FTO substrate and the mesoporous TiO_2 film (especially in trial solid-state cells). In systems with such a blocking layer tunnel currents might still play a role under special conditions.

Acknowledgment. S.R. acknowledges the financial support provided by the Minerva Foundation and the European Union's Human Potential Program under contract HPRN-CT-2000-00141, ETA Solar Cells.

References and Notes

(1) O'Regan, B.; Grätzel, M. *Nature* **1991**, *353*, 737.

(2) Kumara, G. R. A.; Kaneko, S.; Okuya, M.; Tennakone, K. *Langmuir* **2002**, *18*, 10493.

(3) Kumara, G. R. A.; Konno, A.; Shiratsuchi, K.; Tsukahara, J.; Tennakone, K. *Chem. Mater.* **2002**, *14*, 954.

(4) Zhang, X. T.; Liu, H. W.; Taguchi, T.; Meng, Q. B.; Sato, O.; Fujishima, A. *Sol. Energy Mater. Sol. Cells* **2004**, *81*, 197.

(5) Schwarzburg, K.; Willig, F. *J. Phys. Chem. B* **1999**, *103*, 5743.

(6) Ferber, J.; Luther, J. *J. Phys. Chem. B* **2000**, *105*, 4895.

(7) Kron, G.; Rau, U.; Werner, J. H. *J. Phys. Chem. B* **2003**, *107*, 13258.

(8) Asbury, J. B.; Hao, E.; Wang, Y.; Ghosh, H. N.; Lian, T. *J. Phys. Chem. B* **2001**, *105*, 4545.

(9) Hagfeldt, A.; Grätzel, M. *Chem. Rev.* **1995**, *95*, 49.

(10) The concentrations normally used in DSSCs are about 0.5 and 0.05 M and thus equal to $\sim 3 \times 10^{20}$ and $\sim 3 \times 10^{19}$ cm^{-3}, respectively. Under steady-state operation there is about one mobile electron/TiO_2 particle. This yields around 10^{18} cm^{-3} for commonly used TiO_2 particles with a diameter of approximately 20 nm and a film porosity of 50%.

(11) Schlichthörl, G.; Huang, S. Y.; Sprague, J.; Frank, A. J. *J. Phys. Chem. B* **1997**, *101*, 8141.

(12) Södergren, S.; Hagfeldt, A.; Olsson, J.; Lindquist, S. E. *J. Phys. Chem.* **1994**, *98*, 5552.

(13) Cahen, D.; Hodes, G.; Grätzel, M.; Guillemoles, J. F.; Riess, I. *J. Phys. Chem. B* **2000**, *104*, 2053.

(14) Kron, G.; Egerter, T.; Nelles, G.; Yasuda, A.; Werner, J. H.; Rau, U. *Thin Solid Films* **2002**, *403*−*404*, 242.

(15) Bisquert, J.; Garcia-Belmonte, G.; Fabregat-Santiago, F. *J. Solid State Electrochem.* **1999**, *3*, 337.

(16) Pichot, F.; Gregg, B. A. *J. Phys. Chem. B* **1999**, *104*, 6.

(17) Kron, G.; Egerter, T.; Werner, J. H.; Rau, U. *J. Phys. Chem. B* **2003**, *107*, 3556.

(18) Bastide, S.; Gal, D.; Cahen, D.; Kronik, L. *Rev. Sci. Instrum.* **1999**, *70*, 4032.

(19) A previously proposed band diagram (ref 13, Figure 4) used a slightly larger value for the redox potential and was constructed on the assumption that the intrinsic properties of the mesoporous TiO_2 play a dominant role. This led to an accumulation layer in the TiO_2 film close to the FTO substrate.

(20) Simmons, J. G. *J. Appl. Phys.* **1963**, *34*, 2581.

(21) Equation 2 was derived for $T = 0$ K. A closed form expression for tunnel currents for $T > 0$ has been presented in the literature for systems with thermally activated electrons, distributed closely around the Fermi level. The difference between the tunnel current at absolute zero and room temperature is less than 5% for electron barrier widths of about 1 nm [ref 22], which we consider, so that the tunnel current expression at absolute zero was used, for the sake of simplicity.

(22) Simmons, J. G. *J. Appl. Phys.* **1964**, *35*, 2655.

(23) Bisquert, J.; Cahen, D.; Hodes, G.; Rühle, S.; Zaban, A. *J. Phys. Chem. B* **2004**, *108*, 8106.

(24) van de Krol, R.; Goossens, A.; Meulenkamp, E. A. *J. Appl. Phys.* **2001**, *90*, 2235.

(25) Cameron, P.; Peter, L. M. *J. Phys. Chem. B* **2003**, *107*, 14394.